Space and time behaviour of the temperature second-order structure function in Rayleigh-Bénard convection

2016 J. Phys.: Conf. Ser. 708 012007

(http://iopscience.iop.org/1742-6596/708/1/012007)

Journal of Physics: Conference Series **708** (2016) 012007 doi:10.1088/1742-6596/708/1/012007

Space and time behaviour of the temperature second-order structure function in Rayleigh-Bénard convection

Riccardo Togni[1], Andrea Cimarelli[1,2], Adrián Lozano-Durán[3] and Elisabetta De Angelis[4]

[1]DIN, Università di Bologna, Via Fontanelle 40, 47121 Forlì, Italy
[2]DISMI, Università degli Studi di Modena e Reggio Emilia, Via Giovanni Amendola 2, 42122 Reggio Emilia, Italy
[3]School of Aeronautics, Universidad Politécnica de Madrid, 28040 Madrid, Spain
[4]School of Engineering - Cardiff University, Queen's Buildings, The Parade, Cardiff, CF24 3AA, United Kingdom

E-mail: DeAngelisE@cardiff.ac.uk

Abstract. One of the most peculiar aspects of turbulence in wall bounded-flows is the ability of the turbulent fluctuations to regenerate themselves through self-sustained processes. The dynamics of these self-sustaining mechanisms has been extensively investigated in the past via two complementary approaches. From one side, the possibility to identify very robust kinematic features within the flow feeds the hope of the scientific community to obtain a complete and consistent dynamical description of the physics of the turbulent regeneration cycles in terms of the so-called coherent structures. From the other side, the multi-scale and inhomogeneous features of the self-sustaining mechanisms of turbulence have been addressed by means of global statistical quantities based on two-point averages such as second-order structure functions. The present work attempts to link these two approaches, by identifying how turbulent cycle mechanisms and turbulent structures reflect on the global statistical properties of second-order structure function. To this aim we use Direct Numerical Simulation data of thermally driven turbulence in the Rayleigh-Bénard convection and we analyse for the first time the behaviour of the second-order structure function of temperature in the complete four-dimensional space of spatio-temporal scales and wall-distances. The observed behaviour is then interpreted in terms of the dynamics of coherent thermal structures and of their commonly accepted model of life-cycle.

1. Introduction

A fundamental concept of turbulence theory is represented by the multi-scale scenario introduced by Richardson [1] and further developed by Kolmogorov [2]. At sufficiently high Reynolds numbers and away from the boundaries or other singularities, a clear distinction between large and small scales can be made. Large eddies are directly influenced by the geometry of the flow, whereas the behaviour of the small ones is almost universal as it depends only on the rate at which they receive energy and on viscosity. The latter represents one of the few exact and nontrivial results in the field of turbulence, nevertheless the limitations of the leading hypotheses makes this framework a particular case, although conceptually of invaluable importance [3].

In the next few decades after Kolmogorov [4, 5] until this day [6, 7, 8, 9], many research groups have spent a lot of efforts trying to understand and model turbulence. However, even if the same goal is shared by all these groups, the methodologies adopted are very different, which lead sometimes to contradicting results. Historically, turbulence has been approached in a *statistical* and in a *structural* sense. The decomposition introduced by Reynolds represents the first attempt to describe turbulence in a statistical way by splitting the field into an average component and a fluctuating one [10]. On the other side, Richardson was the pioneer of the structural approach by portraying turbulence in terms of eddies of different sizes [1].

Loosely speaking, the statistical point of view deals with the global statistics of the turbulent flow field whereas the structural one considers turbulence as a property of deterministic solutions of the governing equations rather than as a stochastic process [11]. While in the structural approach the results obtained are mainly influenced by the choice of the eduction technique (e.g. quadrant analysis [12], VITA [13], POD [14], based on invariants of the velocity-gradient tensor [15], etc.), in the statistical one the results depend only on the choice of the observable (e.g. mean velocity, turbulent intensities, etc.). Quantitatively the results of these two approaches are not comparable but they can complement each other and the results obtained by one method can support or clarify the evidences obtained by the other.

The aim of the present work is to try to bridge the gap between these two approaches by searching possible explanations of the behaviour shown by the second-order structure function in the different features shown by turbulent structures. To this purpose we use the Rayleigh-Bénard convection, see Ref. [16] for a recent review. In such a flow, thermally driven turbulence shows a much more coherent pattern with respect to more classical pressure-driven wall-turbulence. Indeed, the turbulent cycle is characterized by one single coherent structure, the so-called thermal plume. The prominent role played by thermal plumes is then expected to leave a marked footprint on global statistical quantities. Indeed, we here propose the analysis of the second-order structure function for the temperature field. To further increase the possibility of recognize features related to turbulent structures on the behaviour of second-order structure function, we address here for the first time, the entire augmented-space of wall-turbulence, i.e. the compound space of spatial and temporal scales and wall-distances. Needless to say this study represents only a first step toward a more complete analysis represented by the Yaglom equation, i.e. the balance for the second order structure function, where the study of the different ranges of scales and positions encountered by the related fluxes endows the second-order moment with its physical interpretation.

2. Direct Numerical Simulation

The Rayleigh-Bénard convection (RBC) consists of a fluid layer heated from below and cooled from above by two horizonatal plates in a laterally unbounded domain. The governing equations for RBC are the continuity, Navier-Stokes and energy equations under the Boussineq approximation

$$\begin{aligned}
&\frac{\partial u_i}{\partial x_i} = 0, \\
&\frac{\partial u_i}{\partial t} + \frac{\partial u_i u_j}{\partial x_j} = -\frac{\partial p}{\partial x_i} + \sqrt{\frac{Pr}{Ra}}\frac{\partial^2 u_i}{\partial x_j \partial x_j} + \theta\delta_{i2}, \\
&\frac{\partial \theta}{\partial t} + \frac{\partial \theta u_j}{\partial x_j} = \frac{1}{\sqrt{PrRa}}\frac{\partial^2 \theta}{\partial x_j \partial x_j},
\end{aligned} \tag{1}$$

where $i, j = 1, 2, 3$, δ_{ij} is the Kronecker delta and the variables u_i, p, θ are respectively the velocity, pressure and temperature fields. We introduce the commonly-used spatial coordinates $x = x_1$, $y = x_2$, $z = x_3$ and velocity components $u = u_1$, $v = u_2$, $w = u_3$. The Cartesian coordinate system is cell-centered, with the xz-plane parallel to the horizontal plates and the y-axis pointing in the direction opposite to that of gravity acceleration, see figure 1. Equations

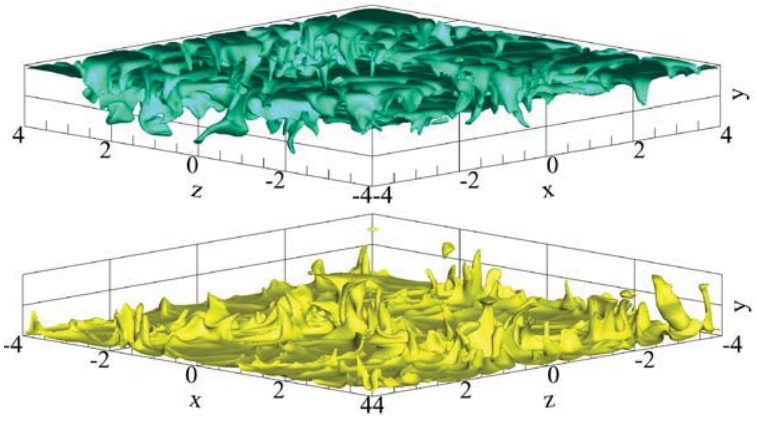

Figure 1. Isosurfaces of temperature ($\theta = 0.3$ down and $\theta = -0.3$ up) for $Ra = 1.0 \times 10^6$.

(1) are written in a dimensionless form using the distance between the plates H, the temperature difference between the lower and the upper plates $\Delta\Theta$ and the free-fall velocity $U_f = \sqrt{g\alpha\Delta\Theta H}$ as characteristic scales, where g and α are the gravity acceleration and the thermal expansion coefficient respectively. In what follows, all the results will be reported in a non-dimensional form by using H, $\Delta\Theta$ and U_f as characteristic quantities. The resulting non-dimensional groups are the Prandtl $Pr = \nu/\kappa$ and Rayleigh numbers $Ra = g\alpha\Delta\Theta H^3/\nu\kappa$, where ν the kinematic viscosity and κ the thermal diffusivity. The Boussinesq equations (1) are solved using a pseudospectral method which discretizes space with Chebychev polynomials in the y direction and with Fourier modes in the x and z directions. Time integration is performed with a fourth-order Runge-Kutta scheme for the nonlinear terms and a Crank-Nicholson scheme for the linear ones. Two DNS are performed for $Pr = 0.7$ at $Ra = 1.7 \times 10^5$ and 1.0×10^6 in a rectangular box of sizes $L_x = 8$, $L_y = 1$, $L_z = 8$. Periodic boundary conditions are imposed at the lateral sidewalls whereas isothermal and no-slip boundary conditions are used on the top and bottom plates. This rather large computational domain has been considered, at the expense of the Ra values reachable, in order to analyze the second-order structure function without being influenced by the horizontal periodicity. The DNS at $Ra = 1.7 \times 10^5$ and at $Ra = 1.0 \times 10^6$ employ $128 \times 129 \times 128$ and $256 \times 129 \times 256$ dealiased modes and polynomials respectively, see Ref. [17] for further details about the simulations and for the validation of the dataset.

3. Flow structures in thermally driven turbulence

Let us now briefly describe the topology of the flow. The turbulence regeneration cycle of RBC is composed by coherent thermal and velocity structures which emerge from the chaotic regime, combine themselves and create a sort of persistent machinery. The most relevant coherent structure that can be identified in this cycle is the so-called *thermal plume*, which can be loosely defined as a portion of fluid having a temperature difference with respect to the background [16] (see figure 2(a)). These structures follow a precise life-cycle [18], in particular hot and cold plumes detach from the bottom and the upper plate respectively, move throughout the fluid layer driven by buoyancy force and finally impinge on the opposite wall triggering the ejection of new plumes [17]. In the core, thermal plumes have a mushroom-like shape whereas close to the walls they have a sheet-like one, see figure 1. Generally speaking, the sheet-like plumes create a fine network across the plates and the mushroom-like plumes are emitted from the intersection spots [19]. Both the ejection and impingement events of plumes take place not at the wall, but approximately on the edge of a conductive layer, made of quiescent fluid, called *thermal*

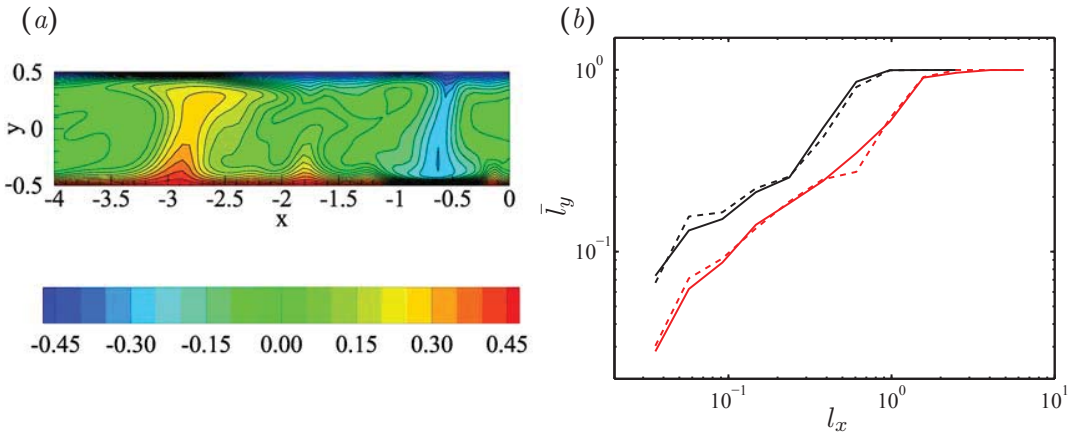

Figure 2. (a) Vertical section of the fluid domain colored with the temperature at $Ra = 1.7 \times 10^5$. (b) Mean wall-normal length, $\bar{l}_y$, as a function of the streamwise lengths of the structures l_x. Solid and dashed lines for high- and low-temperature structures respectively. Colors are black for $Ra = 1.7 \times 10^5$ and red for $Ra = 1.0 \times 10^6$.

boundary layer. The thermal boundary layer thickness δ_θ is usually defined by considering a thickness based on the slope of the mean temperature profile

$$\delta_\theta = \frac{1}{2}\left(\left|\frac{d\Theta}{dy}\right|_{y=y_{wall}}\right)^{-1} = \frac{1}{2Nu}, \tag{2}$$

where Θ is the mean temperature and Nu is the Nusselt number. The Nusselt number for $Ra = 1.7{\times}10^5$ is equal to 5.0 whereas for $Ra = 1.0{\times}10^6$ is equal to 8.2 [17]. It is worth noting that also large-scale circulations are found to characterize thermally driven turbulence with different features according to the geometry of the domain [20, 21, 22]. In doubly-periodic rectangular geometries, the large-scale circulation is found to be composed by ascending and descending plumes locking into a roll-like structure; the latter undergoes a continuous displacement along the horizontal directions x, z and exhibits a quite persistence in time [21].

To further address the topology of the flow we use now a thresholding technique similar to the one adopted in [23] and [9] in order to identify scalings of properly defined three-dimensional high- and low-temperature structures. We consider temperature structures the connected region of the flow such that $|\theta'(x,y,z)| > \alpha\theta'_{rms}(y)$, where θ' is the fluctuating temperature, α a thresholding parameter, and $\theta'_{rms}(y)$ the root-mean-square of the fluctuating temperature as a function of the wall-normal coordinate. As apparent, the resulting set of structures depends on the value of the threshold. By means of a percolation analysis, we select a threshold, $\alpha = 1.5$, which is found to maximize the number of identified structure. Every single object is also classified as a high- or low-temperature structure according to the sign of θ'_m computed over the domain Ω of all its constituent points as,

$$\theta'_m = \frac{\int_\Omega \theta'(x,y,z)dV}{\int_\Omega dV}. \tag{3}$$

The above procedure yields about 10^3 objects for $Ra = 1.7 \times 10^5$ and 4×10^3 for $Ra = 1.0 \times 10^6$. In order to characterize this population, we circumscribe each structure in a box aligned to the Cartesian axes, whose streamwise, wall-normal and spanwise sizes are denoted by l_x, l_y and l_z. This procedure allows us to characterize in a more quantitative way the structural properties

of the temperature field. Indeed, as expected, we found that these objects are characterized by having roughly the same horizontal lengths, $\bar{l}_x \sim l_z$ and $\bar{l}_z \sim l_x$ where $\bar{\cdot}$ denotes the ensemble average over the population of identified thermal structures. The analysis of the $(l_x, \bar{l}_y)$-space shown in figure 2(b) reveals the presence of a hierarchy of thermal structures whose sizes satisfy $\bar{l}_y \sim l_x$. The results also show that there are many structures spanning the full height, $\bar{l}_y \sim 1$. It is worth underlining the fact that this specific result might reasonably change when higher Rayleigh numbers are addressed. This analysis can be also extended by considering a tracking of the time evolution of these objects thus fully exploiting the potentiality of the approach.

4. The four-dimensional augmented-space of thermally driven turbulence

It is well-known that turbulence is a phenomenon characterized by fluctuations occurring at many space and time scales [24]. Beyond the intuitive idea which arises from observation, a *scale* of turbulence is quite an elusive quantity which is not univocally defined. From a statistical point of view, the scale of a turbulent field can be defined by using second-order structure function as the separation vector between two points and two times. The second-order structure function for a generic quantity β can be written as

$$\left\langle \delta\beta^2 \right\rangle = \left\langle \delta\beta\delta\beta \right\rangle , \tag{4}$$

where

$$\delta\beta = \beta' \left(X_{cj} + r_j/2, T_c + \tau/2 \right) - \beta' \left(X_{cj} - r_j/2, T_c - \tau/2 \right) \tag{5}$$

denotes the increment of the fluctuations β' between the point $X_{cj} - r_j/2$ at time $T_c - \tau/2$ and the point $X_{cj} + r_j/2$ at time $T_c + \tau/2$. Thus, the second-order structure function (4) depends on the spatial separation vector r_i, on the spatial location of the mid-point X_{ci}, on the temporal separation τ and on the temporal location of the mid-time T_c. Due to the statistical symmetries of RBC in both space and time, the dependence on the mid-point X_{ci} reduces simply to the distance from the wall $Y_c = X_{c2}$ whereas the dependence on the mid-time T_c vanishes. Furthermore, by accounting for the statistical isotropy in the horizontal planes, the functional dependence of $\left\langle \delta\beta^2 \right\rangle$ on $(r_x, r_y, r_z, \tau, Y_c)$ reduces to (r_π, r_y, τ, Y_c), where $r_\pi = \sqrt{r_x^2 + r_z^2}$. It is worth noting that, the r_y direction is limited by the presence of the wall, i.e. wall-normal scales cannot extend for a distance greater than twice the distance of the mid-point from the wall, $r_y \leq 2Y_c$ [25].

As previously mentioned, the most relevant coherent structure that can be identified in RBC, for Rayleigh numbers sufficiently above the onset of convection [26], is the so-called thermal plume. In accordance with the definition outlined above, plumes are coherent structures of temperature rather than being structures of momentum, therefore their statistical footprint is mostly marked on observables built with the temperature field. For this reason, we analyze the behaviour of the second-order structure function of temperature $\left\langle \delta\theta^2 \right\rangle$ as a function of (r_π, r_y, τ, Y_c). This statistical observable can be considered a measure of the temperature variance of turbulence at a scale (r_π, r_y, τ) and at a position Y_c, thus it will be hereafter called also *scale variance*. For the sake of statistical convergence, two sets of uncorrelated time-series are collected, one for $Ra = 1.7 \times 10^5$ (14 time-series) and another for $Ra = 1.0 \times 10^6$ (7 time-series). Being $2H/U_f$ the dimensional large eddy turnover time and $\tau_\ell = 2$ its non-dimensional value, these time series are $2.5\tau_\ell$ long within which 51 samples are collected to compute two-points and two-times statistics.

5. Results

Figure 3(a) and (b) show the isocontours of the scale variance $\left\langle \delta\theta^2 \right\rangle$ in the reduced (r_π, r_y, τ)-space for $Y_c = 0.1$, $Y_c = 0.3$ at $Ra = 1.7 \times 10^5$. The planes colored with $\left\langle \delta\theta^2 \right\rangle$ are orthogonal and chosen in such a way that they cross the maxima achieved by $\left\langle \delta\theta^2 \right\rangle$ at $Y_c = 0.1$ and $Y_c = 0.3$

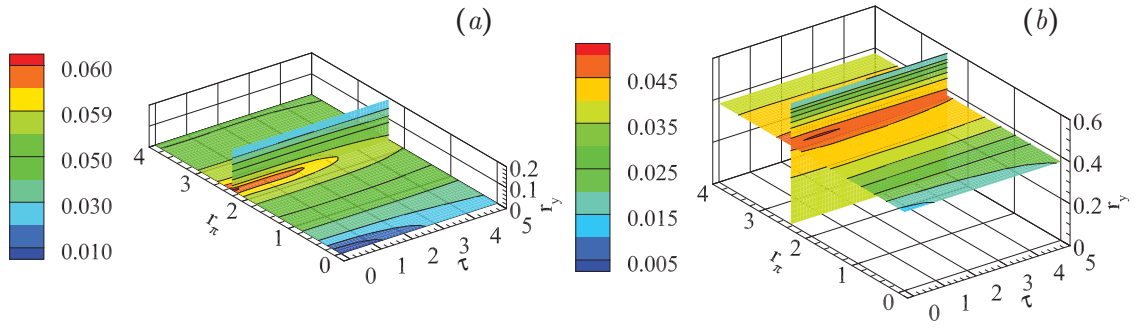

Figure 3. Isocontours of $\langle \delta\theta^2 \rangle$ in the reduced (r_π, r_y, τ)-space at (a) $Y_c = 0.1$ and (b) $Y_c = 0.3$ for $Ra = 1.7 \times 10^5$.

respectively. Around the origin and for both wall-distances, scale variance starts from zero at $r_\pi = r_y = \tau = 0$ and then increases when augmenting the separations in space and time. The location of the maximum, on the other hand, changes depending on the wall-distance; close to the plate for $Y_c = 0.1$, the scale variance is peaked at $r_\pi = 2.4$ and $r_y = \tau = 0$. On the contrary, further away from the wall at $Y_c = 0.3$, the maximum occurs at well-defined scales $r_\pi = 2.4$, $r_y = 0.4$ and $\tau = 1$. The same qualitative behaviour is observed also for the larger Rayleigh number considered.

In order to set quantitatively the behaviour of scale variance, let us consider the Y_c-behaviour of the *characteristic scales* $(\tilde{r}_\pi, \tilde{r}_y, \tilde{\tau})$ defined as the locus of the scale variance maxima at different distances from the plates, i.e.

$$\langle \delta\theta^2 \rangle_{max} (Y_c) = \langle \delta\theta^2 \rangle (Y_c | \tilde{r}_\pi, \tilde{r}_y, \tilde{\tau}) \; .$$

The analysis of $(\tilde{r}_\pi, \tilde{r}_y, \tilde{\tau})$ as a function of Y_c reveals that the horizontal scale $\tilde{r}_\pi$ is almost constant with Y_c. In particular, $\tilde{r}_\pi = 2.4$ for $Ra = 1.7 \times 10^5$ and $\tilde{r}_\pi = 2.7$ for $Ra = 1.0 \times 10^6$. The fact that the characteristic horizontal length remains constant with the distance from the wall means that the most intense temperature fluctuations occur at a specific horizontal scale. Furthermore, it sounds reasonable that $\tilde{r}_\pi$ could be indicative of the average distance between an ascending and a descending hot and cold temperature structure. In support of this conjecture, we can see in figure $2(a)$ that the distance between the hot and the cold plumes for the DNS at $Ra = 1.7 \times 10^5$ is around 2.5, which is quite similar to the correspondent $\tilde{r}_\pi$. An analogous result is reported in Ref. [21], where a symmetry-accounting ensemble-averaging method is employed to identify large-scale rolls in an unbounded RBC at $Ra = 1.0 \times 10^7$ and $Pr = 1$; they found that the distance between ascending and descending fluid is, on average, almost equal to two-times the height of the fluid domain.

Contrary to the horizontal scale, the wall-normal scale is found to be zero close to the plates and to increase linearly with the wall-distance in the core of the flow as shown in figure $4(a)$ and (b). Let us analyse more in detail the linear behaviour of the wall-normal scale in the core of the flow. The maxima of scale variance for each wall-distance are located near the $(r_y = 2Y_c)$-plane. In particular, we measure that the exact plane where the maxima occur is

$$\tilde{r}_y = 2 \left[Y_c - \frac{1}{2Nu} \right] \; ,$$

for both the Rayleigh numbers considered. Hence, these wall-normal scales are representative of thermal fluctuations occurring on scales extending down to a distance from the wall $1/(2Nu)$

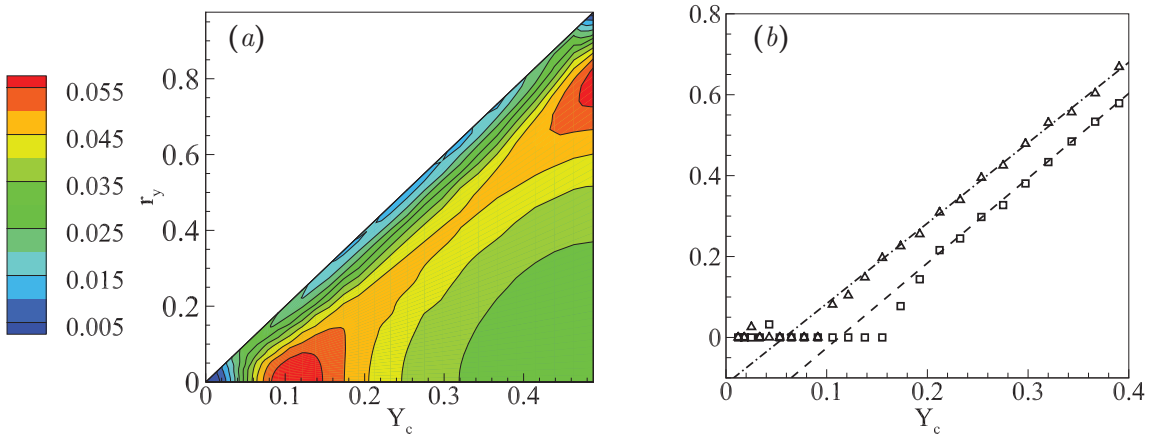

Figure 4. (a) Section of the space (r_π, r_y, τ, Y_c) in the $(r_\pi = 2.4, \tau = 0)$-plane colored with $\langle \delta\theta^2 \rangle$ for $Ra = 1.7 \times 10^5$. (b) Characteristic wall-normal scale $\tilde{r}_y(Y_c)$ as a function of Y_c for $Ra = 1.7 \times 10^5$ (squares) and $Ra = 1.0 \times 10^6$ (triangles). The equation of the dashed line is $2.1(Y_c - 0.12)$ whereas the equation of the dashed-dot line is $2.0(Y_c - 0.06)$.

which is exactly the non dimensional thermal boundary layer thickness defined in (2). Hence, we can claim that the most intense thermal fluctuations are *attached* to the thermal boundary layer. This behaviour may be explained in terms of dynamics of turbulent structures in the following way. Thermal plumes detach from the near-wall region and span the entire domain impinging on the opposite wall but retaining their roots attached to the original wall. On the other hand, both the ejection and the impingement of plumes take place not at the wall, but approximately on the edge of a conductive layer, made of quiescent fluid, the thermal boundary layer. Thus, the overall picture is consistent with attached thermal structure spanning the entire convection cell from one thermal boundary layer to the opposite one.

It is finally interesting to note that, as shown in figure 4, two well-defined peaks of scale variance (colored in red) are present around $Y_c = 1/(2Nu) = 0.1$ for $r_y = 0$, $r_\pi = 2.4$ and $Y_c = 0.5$ for $r_y = 2\,[Y_c - 1/\,(2Nu)]$, $r_\pi = 2.4$, respectively on top of the thermal boundary layer and at the center of fluid layer. Both these two peaks appear to be a footprint of the same temperature structure and to be strongly related with the inhomogeneity of the flow in the vertical direction. In particular, the temperature structure is again a couple of ascending (hot) and descending (cold) fluid statistically separated in the horizontal direction by $r_\pi = 2.4$ and these two peaks are a statistical evidence of the impinging/ejection events. Indeed, as sketched in figure 5, on top of the thermal boundary layer, $Y_c = 1/(2Nu) = 0.1$, the horizontal scale of the maximum is $r_\pi = 2.4$ while the wall-normal scale is zero because at this position non-zero increments, $r_y \neq 0$, would involve the temperature field closer to the plate and, hence, outside the thermal plume. On the contrary, at the channel center, $Y_c = 0.5$, the statistical occurrence of impinging and ejection events of couples of hot/cold plumes appear again for $r_\pi = 2.4$ but for $r_y = 2\,[Y_c - 1/\,(2Nu)]$ which involve exactly the two points lying on top of the two opposite thermal boundary layer where the impinging/ejection events occur, see again sketch 5. As previously mentioned, these aspects are strongly related with the inhomogeneity of the flow. Indeed, by considering increments only in the wall-normal scales, the second-order structure function of temperature can be written as

$$\langle \delta\theta^2 \rangle\,(r_y, Y_c) = \langle \theta'^2 \rangle\,(Y_c + r_y/2) + \langle \theta'^2 \rangle\,(Y_c - r_y/2) - 2\,\langle \theta'\,(Y_c + r_y/2)\,\theta'\,(Y_c - r_y/2) \rangle\,, \qquad (6)$$

thus highlighting the different contributions to the r_y behaviour. It is clear that for large

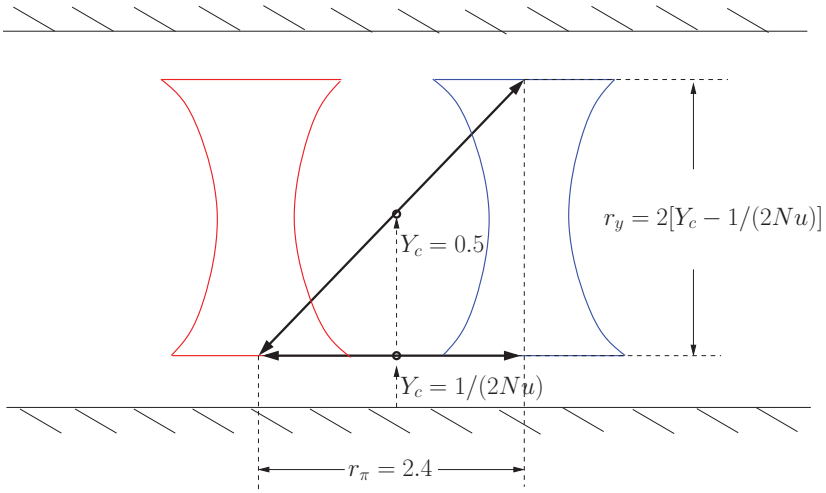

Figure 5. Sketch of the statistical occurrence of ascending (hot) and descending (cold) fluid and of the increments involved in the two maxima of the second-order structure function of temperature occurring on top of the thermal boundary layer $Y_c = 1/(2Nu) = 0.1$ and at the cell center $Y_c = 0.5$. The value $r_\pi = 2.4$ is relative to the $Ra = 1.7 \times 10^5$ case.

separation, the inhomogeneity strongly influences the space of wall-normal scales by setting the locus of the maxima of $\langle \delta\theta^2 \rangle$ in the plane of attached scales, $r_y = 2\,[Y_c - 1/\,(2Nu)]$, via the the spatial distribution of temperature variance given by the first two terms of (6). Since, the maxima of $\langle \delta\theta^2 \rangle$ in the $r_y = 2\,[Y_c - 1/\,(2Nu)]$-plane are here linked with the statistical occurrence of ascending (hot) and descending (cold) plumes being occurring for $r_\pi = 2.4$, we can conjecture that the location of the maximum of temperature variance $\langle \theta^2 \rangle$ at $Y_c = 1/(2Nu)$ and the thickness of the thermal boundary layer δ_θ are settled by the impinging/ejection events of thermal plumes.

Let us now focus on the time scale behaviour of scale variance. In figure 6(a) and (b) the isocontours of $\langle \delta\theta^2 \rangle$ in the $(r_\pi = 2.4, Y_c = 0.1)$-plane and $(r_\pi = 2.4, Y_c = 0.3)$-plane are shown respectively. As previously noted, close to the plates, the maximum of scale variance occurs for $r_\pi = 2.4$ and for $r_y = \tau = 0$. Increasing both r_y and τ a decrease of $\langle \delta\theta^2 \rangle$ is observed. On the contrary, further away from the walls, characteristic scales are observed also in the wall-normal and time scales being present a maximum at attached wall-normal scales and for $\tau > 0$. However, let us notice that while the shape of this maximum is peaked in the wall-normal scales, the temporal behaviour is very smooth thus leading to significant uncertainties on the measurement of $\tilde{\tau}$. The behaviour of the characteristic time scales $\tilde{\tau}(Y_c)$ as a function of the wall-distance is shown in figure 6(c). In the near-wall region no characteristic time scale is defined being $\tilde{\tau}(Y_c) = 0$ in this region of the flow. This aspect actually suggests that the impinging events on top of the thermal boundary layer statistically causes ejection events at the same time, $\tau = 0$, at an horizontal distance $r_\pi = 2.4$, see again sketch 5. Then, as expected, a characteristic time scale, $\tilde{\tau} > 0$, is observed further away from the wall where the maxima of $\langle \delta\theta^2 \rangle$ show an attached behaviour in the wall-normal scales. This time scale is a statistical measure of the time needed by the ejection event created on top of the thermal boundary layer by an impinging event, to reach the wall-distance $y = Y_c + r_y/2$, see sketch 5. In particular, we measure that to reach the cell center $y = Y_c + r_y/2 \sim 0.5$, the thermal structure statistically spends 2 large eddy turnover time τ_ℓ. Then, for $Y_c > 0.33$, the time scale $\tilde{\tau}$ drops to zero. This aspects can be associated to the fact that the impinging event that created the ejection statistically vanishes

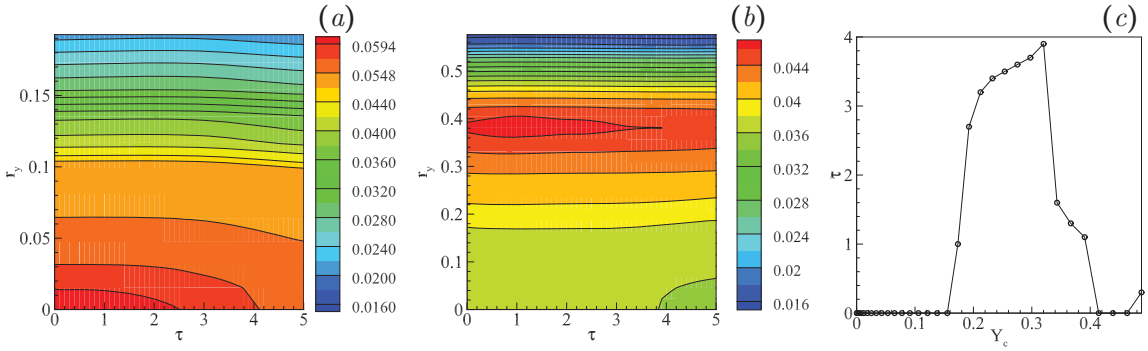

Figure 6. Section of the space (r_π, r_y, τ, Y_c) in the (a) $(r_\pi = 2.4, Y_c = 0.1)$-plane and (b) $(r_{pi} = 2.4, Y_c = 0.3)$-plane colored with $\langle \delta\theta^2 \rangle$ for $Ra = 1.7 \times 10^5$. (c) Characteristic time scale $\tilde{\tau}(Y_c)$ as a function of Y_c for $Ra = 1.7 \times 10^5$.

after 2 large eddy turnover times which is the time employed by the ascending plume to reach the wall-distance $y = Y_c + r_y/2 \sim 0.5$. However, further investigation accounting for a longer range of time scales is mandatory to draw a conclusion with any certainty. Indeed, it would be also possible that, at these wall-distances, the characteristic time scale exceeds the maximum time scale here analysed.

6. Conclusions

Direct Numerical Simulation data of turbulent Rayleigh-Bénard convection are analysed for the first time in terms of second-order structure function of the temperature field in the complete four-dimensional augmented space of spatial and temporal scales and wall-distances. The observed behaviour for the second-order structure function is then clarified from a dynamical point of view by means of the commonly accepted model of life-cycle for the thermal structures. The second-order structure function shows marked maxima for a fixed horizontal length scale at different wall-distances that is found to be related with the average distance between a couple of ascending (hot) and descending (cold) thermal structures. This length is Rayleigh dependent and is found to be $r_\pi = 2.4$ and 2.7 for $Ra = 1.7 \times 10^5$ and $Ra = 1.0 \times 10^6$, respectively. The life-cycle of thermal structures is found to leave a clear footprint also in the wall-normal scales. Indeed, we found that $\tilde{r}_y = 2\,[Y_c - 1/\,(2Nu)]$ highlighting the fact that the most intense thermal fluctuations occur at scales extending down to the edge of the thermal boundary layer in agreement with the commonly accepted model for the dynamics of plumes [18]. We also found that the statistical occurrence of an impinging event on top of the thermal boundary layer is related with the simultaneous appearance of an ejection event at an average horizontal distance $r_\pi = 2.4$ and 2.7 respectively for the $Ra = 1.7 \times 10^5$ and $Ra = 1.0 \times 10^6$ cases. The resulting ejection of fluid is found to spend 2 large eddy turnover time τ_ℓ to reach the cell center. Afterwards, the impinging event which created it vanishes thus highlighting that the life-time of impinging is 2 large eddy turnover time τ_ℓ. The results presented in this work surely justify a deeper analysis of the problem and the very next step will be investigating more turbulent systems at higher Rayleigh numbers.

Acknowledgments

The authors would like to acknowledge the support of the European Research Council, which funded the Multiflow summer program within which this work was developed.

References

[1] Richardson L F 1922 Weather prediction by numerical process (Cambridge U. Press)
[2] Kolmogorov A N 1941 Dissipation of energy in locally isotropic turbulence *Dokl. Akad. Nauk SSSR* **32** 19–21
[3] Pope S B 2000 Turbulent flows (Cambridge U. Press)
[4] Monin A S and Yaglom A M 1971 Statistical Fluid Mechanics: Mechanics of Turbulence, Volume 1 (MIT Press, Cambridge, MA)
[5] Townsend A A 1976 The structure of Turbulent Shear Flow (Cambridge U. Press)
[6] Chong M S, Perry A E and Cantwell B J 1990 A general classification of three-dimensional flow fields *Phys. Fluids A* **2** 765–777
[7] Domaradzki J A and Rogallo R S 1990 Local energy transfer and nonlocal interactions in homogeneous, isotropic turbulence *Phys. Fluids A* **2** 413–426
[8] Cimarelli A and De Angelis E 2014 The physics of energy transfer toward improved subgrid-scale models *Phys. Fluids* **26** 055103
[9] Lozano-Durán A and Jiménez J 2014 Time-resolved evolution of coherent structures in turbulent channels: characterization of eddies and cascades *J. Fluid Mech.* **759** 432–471
[10] Reynolds, O. 1894 On the dynamical theory of incompressible viscous fluids and the determination of the criterion *Proc. R. Soc. Lond.* **56** 40–45
[11] Jiménez J 2013 Near-wall turbulence *Phys. Fluids* **25**, 101302.
[12] Willmarth W W and Lu S S 1972 Structure of the Reynolds stress near the wall *J. Fluid Mech.* **55** 65–92
[13] Blackwelder R F and Kaplan R E 1976 On the wall structure of the turbulent boundary layer *J. Fluid Mech.* **76** 89–112
[14] Berkooz G, Holmes P and Lumley J L 1993 The proper orthogonal decomposition in the analysis of turbulent flows *Annu. Rev. Fluid Mech.* **25** 539–575
[15] Jeong J, Hussain F, Schoppa W and Kim J 1997 Coherent structures near the wall in a turbulent channel flow *J. Fluid Mech.* **332** 185–214
[16] Chillà F and Schumacher J 2012 New perspectives in turbulent Rayleigh-Bénard convection *Eur. Phys. J. E* **35** 1–25
[17] Togni R, Cimarelli A and De Angelis E 2015 Physical and scale-by-scale analysis of Rayleigh-Bénard convection *J. Fluid Mech.* **782** 380–404
[18] Kadanoff L P 2001 Turbulent heat flow: structures and scaling *Phys. Today* **54** 34–39
[19] Zhou Q, Sun C and Xia K Q 2007 Morphological evolution of thermal plumes in turbulent Rayleigh-Bénard convection *Phys. Rev. Lett.* **98** 074501
[20] Niemela J J, Skrbek L, Sreenivasan K R and Donnelly R J 2001 The wind in confined thermal convection *J. Fluid Mech.* **449** 169–178
[21] Van Reeuwijk M, Jonker H J J and Hanjalić K 2005 Identification of the wind in Rayleigh-Bénard convection *Phys. Fluids* **17** 051704
[22] Bailon-Cuba J, Emran M S and Schumacher J 2010 Aspect ratio dependence of heat transfer and large-scale flow in turbulent convection *J. Fluid Mech.* **655** 152–173
[23] Lozano-Durán A, Flores O and Jiménez J 2012 The three-dimensional structure of momentum transfer in turbulent channels *J. Fluid Mech.* **694** 100–130
[24] Frish U 1995 Turbulence: the legacy of A. N. Kolmogorov (Cambridge U. Press)
[25] Cimarelli A, De Angelis E, Talamelli A, Casciola C M and Jiménez J 2014 The attached reverse and detached forward cascades in wall-turbulent flows *J. Phys. Conf. Seri.* **506** 012005
[26] Ahlers G 2009 Trend: Turbulent convection *Physics* **2** 74 (Am. Phys. Soc.)